Materials Science & Engineering A 822 (2021) 141686

Contents lists available at ScienceDirect

Materials Science & Engineering A

journal homepage: www.elsevier.com/locate/msea

A new approach to thermo-mechanical treatment of steel T91 by multiple upsetting-extrusion in a ferritic range

Victor N. Voyevodin [a,b,*], Mikhail A. Tikhonovsky [a], Hanna Yu Rostova [a], Alexander S. Kalchenko [a], Igor V. Kolodiy [a], Natalya F. Andrievskaya [a], Vladimir S. Okovit [a], Marta Serrano [c], Rebeca Hernandez [c], Oleksiy M. Velikodnyi [a], Anastasia V. Levenets [a]

[a] National Science Center Kharkov Institute of Physics and Technology, 1, Akademicheskaya Str, Kharkiv, 61108, Ukraine
[b] V.N. Karazin Kharkiv National University, 4, Svobody Sq., Kharkiv, 61022, Ukraine
[c] Centro Investigaciones Energéticas, Medioambientales y Tecnológicas, 40, Complutense Av., 28040, Madrid, Spain

ARTICLE INFO

Keywords:
Ferritic-martensitic steel T91
Severe plastic deformation
Thermal treatment
Nanostructure
Thermal stability
Mechanical properties

ABSTRACT

The microstructure and mechanical properties of the ferritic-martensitic steel T91 after severe plastic deformation (SPD) and subsequent thermal treatment are investigated. SPD was realized by the method of multiple "upsetting-extrusion" (MUE) in temperature range of stability of ferritic phase (750-575 °C), thermal treatment of SPD specimens was carried out at temperatures 550–730 °C during 1–100 h. It is revealed that decrease of temperature of "upsetting-extrusion" and increase of cycle number to 5 induces the decrease of mean grain size to 145 nm and increase of degree of microstructure homogeneity. At the same time microhardness increases from 1800 MPa to 2850 MPa. Composition, shape, size and density of carbide precipitates in steel after SPD and thermal treatment are determined. Obtained submicron grain ferritic microstructure with high value of microhardness is stable at exposure temperature of 550 °C. It is shown that temperature variation of thermal treatment induces the considerable change in grain size and mechanical characteristics.

1. Introduction

Ferritic-martensitic steels containing 9–12% of chromium (9–12 Cr F/M steels) have lower thermal expansion and higher thermal conductivity compared to austenitic steels of type 316 and 304. Also they have significant corrosion resistance, high temperature strength and heat resistance, as well as high radiation resistance. Due to these properties 9-12Cr F/M steels are considered as a promising material for use in nuclear and thermonuclear reactors of a new generation [1–4]. F/M steels such as EUROFER (Europe), ORNL (USA), F82 N (Japan), CLAM (China), RUSFER-EK-181 (Russia) and others have been developed in various countries. Chromium concentration in most of these steels is about 9%. T91 steel, which was originally designed for use in thermal power energy, also refers to this class of promising materials [5,6].

The determining parameters for its successful use in this field are the high radiation resistance and mechanical properties. Factors which can influence the improvement of these characteristics are composition optimization by microalloying, decreasing the width of martensite laths and grain size as well as number, sizes and homogeneity of distribution of secondary phases [2–4,7]. As it is known, in 9Cr–1Mo steels the secondary phases are typically represented by the $M_{23}C_6$ -type carbides (where M – is mainly Cr) and MX-type carbides (or carbonitrides) (where M – Nb, V or their mixture and X–C, N or their mixture [7–9]).

Composition optimization by the microalloying with appropriate elements improves the mechanical characteristics by increasing the solid solution hardening [10], reducing the grain size and volume fraction of $M_{23}C_6$ carbides with simultaneous increasing of the MX carbonitrides fraction [11]. However, it is not always possible to improve mechanical properties by microalloying, in particular due to the appearance of unwanted secondary phases, especially in the process of long-term operation [12].

Optimization of the thermal treatment (TT) parameters, such as normalization temperature, temperature and time of tempering also improves the structural parameters and properties of F/M steels. The

* Corresponding author. National Science Center Kharkov Institute of Physics and Technology, 1, Akademicheskaya str., Kharkiv, 61108, Ukraine.
E-mail addresses: voyev@kipt.kharkov.ua (V.N. Voyevodin), tikhonovsky@kipt.kharkov.ua (M.A. Tikhonovsky), rostova@kipt.kharkov.ua (H.Y. Rostova), kalchenko@kipt.kharkov.ua (A.S. Kalchenko), kolodiy@kipt.kharkov.ua (I.V. Kolodiy), marta.serrano@ciemat.es (M. Serrano), rebeca.hernandez@ciemat.es (R. Hernandez), velikodnyi@kipt.kharkov.ua (O.M. Velikodnyi), avlevenets@gmail.com (A.V. Levenets).

https://doi.org/10.1016/j.msea.2021.141686
Received 31 March 2021; Received in revised form 27 June 2021; Accepted 1 July 2021
Available online 3 July 2021

microstructure refinement occurs, for example, during thermal cycling of martensitic steel near the austenite-ferrite equilibrium temperature [13]. The use of stage heat treatment in CLAM steel, which consists of fast cooling from the austenization temperature of 1050 °C–850 °C, exposure at this temperature for 1 h and subsequent quenching and tempering, allows to reduce the average size of $M_{23}C_6$ precipitates from 150 to 70 nm [14]. These examples illustrate the possibilities of controlling the microstructure of F/M steels by TT methods. Various methods of thermomechanical treatment (TMT) give even greater possibilities for optimization of microstructural parameters and properties of steels.

Among the TMT methods, first of all, it should be noted the ausforming, which consist in the deformation of steel in the region of stability (or metastability) of austenite. Ausforming with subsequent thermal treatment in ferritic region leads to the nucleation of a large number of small and superfine MX carbides (carbonitrides) on defects (dislocations), which are formed as a result of deformation. So, plastic deformation of P91 steel (9Cr–1Mo) by 20% at 900 °C and the subsequent tempering at 740 °C for 45 min led to increase in the density of the MX precipitates by three orders of magnitude compared with the standard heat treatment (quenching from 1040 °C and subsequent tempering at 730 °C for 1 h). In this case, the average size of the MX precipitates decreased by about four times [15].

One of the most effective methods of TMT is the severe plastic deformation (SPD), which allows producing submicrostructured or nanostructured state in steels; this induces the increase of strength characteristics and radiation resistance of steel [16–19]. The combination of this method with thermal treatment allows to optimize parameters of secondary phase's precipitation. SPD by high pressure torsion (HPT) and equal channel angular pressing (ECAP) are the most effective methods for grain refinement [20–22]. The main parameters that determine resulting microstructural state of specimens are the temperature of SPD and the degree of plastic deformation. HPT of martensitic steel (10 rotations under pressure of 6 GPa) induced the formation of equiaxial grain structure with average size of 140 nm in the case of deformation at room temperature and 200 nm in the case of deformation at 300 °C [20]. The volume fraction of secondary phases decreased in several times, that is, "deformation dissolution" occurred and microhardness of specimens increased twice. SPD of steel T91 in ferritic state by the ECAP method showed that double extrusion of specimens at temperature of 700 °C (the true deformation e = 2.3) induced the crucial decrease in average grain size from 5 μm to 500 nm [21]. Decreasing in temperature of extrusion to 300 °C led to formation of grain size equal to 350 nm and microhardness increasing from ~2.5 GPa to ~3.8 GPa. Deformation of steel T91 by the ECAP method at room temperature showed that after 6 passes (real or equivalent deformation was ~3.8) initial lath martensitic microstructure was completely destroyed and equiaxial grains with size of 200 nm were formed. Tensile strength increased from 730 MPa in the initial state to 1160 MPa [22].

Unfortunately due to the technological peculiarities HPT and ECAP methods, which effectively refine the grain, don't allow to realize SPD of large industrial pieces and are mainly used for producing the experimental specimens. To refine grain structure and improve mechanical properties of F/M steel authors [23] used more technological method of cold rotary forging with subsequent heat treatment. With a decrease in the billet diameter from 22 mm to 5.4 mm (e ~ 2.8) and annealing at 700 °C for 30 min, an ultrafine-grained ferritic microstructure with a grain size of ~270 nm was obtained in the steel, which possesses enhanced mechanical properties. However, the use of this method (in contrast to ECAP, for example) led to significant changes in the sample dimensions.

In present paper we used severe plastic deformation to control microstructure of T91 F/M steel by the method of multiple "upsetting-extrusion" (MUE) developed at NSC KIPT [24,25]. This method proved to be effective for production of ultrafine-grained materials in laboratory and industrial conditions (in this case the diameter of samples can vary from 20 mm to 250 mm) [26,27]. Earlier this method was successfully used for production of ultrafine-grained beryllium, tantalum, titanium, zirconium, niobium-titanium and zirconium-niobium alloys [27–29]. The use of this method allowed to accumulate the required degree of plastic deformation while saving the dimensions of samples [29].

Investigation of SPD effect on steel T91 was carried out during the processes of MUE in the temperature range of stability of ferritic and austenitic phases. The proposed paper presents the results of MUE effect in the range of stability of ferrite on grain size, parameters of secondary phases precipitations and mechanical properties of steel. Effect of thermal treatment at various temperatures and exposure time on these characteristics is also studied. Research results obtained during MUE in austenitic range will be presented in another paper.

2. Materials and methods of investigation

T91 steel was produced by INDUSTELL, Belgium (melting: 504/3, heat 82,566–4). Chemical composition of steel according to the manufacturer data is presented in Table 1. Material was supplied as a plate thickness of 40 mm produced by the hot rolling with subsequent thermal treatment. Thermal treatment included normalization at 1040 °C during 30 min with air cooling and subsequent tempering at 730 °C during 60 min with air cooling to room temperature.

Cylinder specimens with diameter and height of 40 mm were produced from the initial billet. The extrusion of specimen at T = 875 °C from diameter 40 mm–20 mm was carried out. Obtained specimens with diameter 20 mm an height 60 mm were subjected to severe plastic deformation by the multiple "upsetting-extrusion" (MUE); such method means multiple operations of upsetting and extrusion on hydraulic press DB 2432A with force of 160 tf (Fig. 1). Real deformation during one cycle of "upsetting-extrusion" was e ~1.6. Five cycles were carried out on successive decrease of deformation temperature from 750 °C during first cycle to 575 °C during the last one. Total real deformation during 5 MUE cycles was e ~8. The choice of extrusion regime with temperature decreasing was conditioned by the necessity to prevent dynamic recrystallization and enhance the effect of the grain refinement. To decrease the temperature difference between container and deformed specimens the first one was heated to temperature ~300 °C. Before deformation specimens were exposed into furnace during 15 min at temperature of deformation. After SPD specimens were subjected to thermal treatment at temperatures 550–730 °C during 15 min up to 100 h. Thermal treatment was carried out in quartz ampoules in argon atmosphere with subsequent air cooling.

Regimes of upsetting-extrusion and subsequent thermal treatments of steel T91 are presented in Table 2.

Microstructural studies were carried out on metallographic inversion microscope Olympus GX51. The fine structure of specimens was studied on transmission electron microscope JEM-2110 (accelerating voltage 200 kV) equipped with scanning attachment BF-STEM JEOL EM-24511 and energy dispersion X-ray microanalyzer JEOL EX-24063 JGP. Specimens for metallographic studies were preliminary encapsulated into bakelite and then grinded on SiC paper (graininess from P120 to P1200) and polished on diamond suspensions with fraction size of 1 and 0.05 μm. To reveal the microstructure Vielle's reagent was used (5 ml of hydrochloric acid, 1 g of picric acid and 100 ml of ethanol). For TEM study plates 0.3 mm thickness were cut out by spark cutting and mechanically thinned to 0.15 mm. The further thinning was carried out by standard jet electropolishing using Tenupol unit at room temperature of electrolyte (electrolyte composition: 80% C_2H_5OH, 10% $HClO_4$, 10% $C_3H_8O_3$, voltage 70 V). Parameters of grain structure and carbide precipitates (mean size d_m and coefficient of size variation k_v of grains and phases) were determined by computer digital treatment of structure images and further data treatment based on the empiric approach in static package SPSS.

X-ray diffraction study was carried out using DRON-2.0 diffractometer in Bragg-Brentano geometry using Co-K_α radiation and scintillation

Table 1
Chemical composition of T91 steel, (%wt).

Fe	Cr	Mo	Mn	Si	V	Ni	Nb	Cu
Bulk	8.76	0.862	0.597	0.317	0.186	0.099	0.073	0.054
Al	**C**	**N**	**P**	**S**	**Sn**	**B**	**Co**	**As**
0.021	0.088	0.003	0.019	0.0006	0.005	0.0001	0.019	0.007

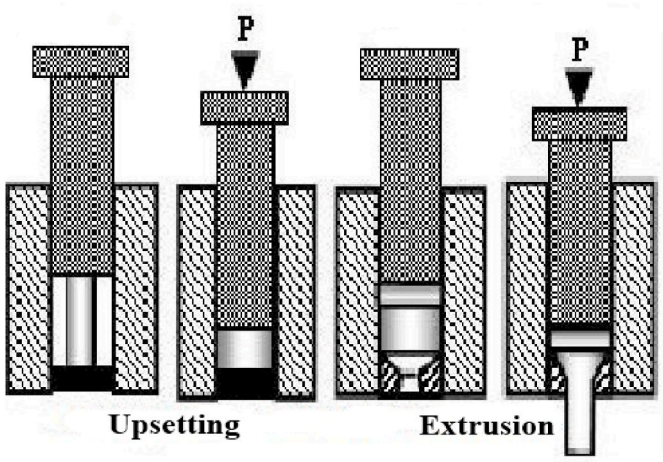

Fig. 1. Schematic diagram of one cycle of "upsetting-extrusion".

Table 2
Regimes of severe plastic deformation and thermal treatment of steel T91.

Code of samples	Regimes of treatment
M-1	As-received state (N&T, normalization 1040 °C, 0.5 h and tempering 730 °C, 1 h
M-2	Extrusion from 40 mm to 20 mm (875 °C, e = 1.5)
M-3	Heating (750 °C, exposure 15 min)
M-4	Extrusion (875 °C, e = 1.5)+3 cycles of UE (750-700-650 °C, e = 4.8)
M-5	Extrusion (875 °C, e = 1.5)+4 cycles of UE (750-700-650-635 °C, e = 6.4)
M-6	Extrusion (875 °C, e = 1.5)+5 cycles of UE (750-700-650-635-575 °C, e = 8.0
M-7	Extrusion (875 °C, e = 1.5)+5 cycles of UE (750-700-650-635-575 °C, e = 8.0)+TT 550 °C
M-8	Extrusion (875 °C, e = 1.5)+5 cycles of UE (750-700-650-635-575 °C, e = 8.0)+TT 600 °C
M-9	Extrusion (875 °C,e = 1.5)+5 cycles of UE (750-700-650-635-575 °C, e = 8.0)+TT 650 °C
M-10	Extrusion (875 °C, e = 1.5)+5 cycles of UE (750-700-650-635-575 °C, e = 8.0)+TT 730 °C

detector. Weight fraction of individual phases (in dual-phase samples) was determined by Rietveld refinement (Maud software). Lattice parameters were calculated by least-square fitting. Estimation of substructure characteristics (crystallite size (CS) D, microstrain ε and dislocations density ρ) is based on diffraction peaks broadening. Analysis was performed by the method proposed in [30]; the main formula is:

$$\beta(s)D = \frac{1}{1 - 4\varepsilon^2/d\beta^2(s)} \quad (1)$$

where β – physical broadening; $s = 2\sin\theta/\lambda = 1/d$; λ – radiation wavelength; θ – diffraction angle; d – interplanar spacing; D – crystallite size; ε – microstrain. Two orders of diffraction peaks (110) and (220) were used for analysis. Silicon powder was used as reference material for calibration of instrumental broadening. Determining of dislocation density was carried out by the formula:

$$\rho = \frac{3\sqrt{2\pi\varepsilon}}{Db} \quad (2)$$

where ρ – dislocation density; b – Burgers vector. For BCC metals and alloys Burgers vector defined as $b = \frac{a}{2} < 111 >$, where a – lattice parameter.

For hardness (Hμ) measurement microhardness tester LM 700 AT was used. The measurement conditions are as follows: load – 200 g, holding time – 14 s. The hardness was measured along the entire surface of the sample section from edge to edge. The minimum number of hardness impress was 10 imprints with a distance of about 4 diagonals of the imprint between them. The measurement error did not exceed 8%. The ImageJ program was used for calculating the density of precipitates. In total, at least 1500 objects were processed on each sample. Mechanical properties of steel T91 (tensile strength σ_B, yield strength σ_τ, elongation δ) were determined by testing of dog-bone specimens with a gage length of 17 mm, width of 2.4 mm and 0.8 mm thickness at a strain rate of 10^{-3} s^{-1} and temperatures from −196 °C to 550 °C. Specimens were mechanically polished to mirror glance before testing. At each temperature three samples were tested and the measurement results were averaged.

3. Results and discussion

3.1. Effect of SPD on structural state of steel

Microstructure of as-received steel T91 (specimen M − 1, Table 2) is typical for tempered martensite and is characterized by the presence of prior austenite grain boundaries and subgrains that are well seen in optical and transmission electron microscopes (Fig. 2). These boundaries are decorated by precipitates of $M_{23}C_6$-type carbides that are always present in steel T91 [15]. The average sizes of prior austenite grains, subgrains and $M_{23}C_6$ precipitates are ~20 μm, ~5 μm and ~125 nm, respectively. Within prior austenitic grains martensitic laths with transverse dimension ~0.25–0.5 μm are observed (Fig. 2b). At high magnification, except rather large $M_{23}C_6$ precipitates, considerable number of fine precipitates with a diameter ≤50 nm is spotted which are always classified as phases of MX type [31–33].

On the diffraction pattern of as-received specimen M − 1 only diffraction peaks of ferrite Fe-α with lattice parameter a = 0.28714 ± $2{\cdot}10^{-5}$ nm (Fig. 3) are observed. Intensity distribution of ferrite peaks corresponds to non-textured state.

The first performed technological operation was extrusion of cylinder billet from diameter 40 mm–20 mm (ε = 1.5) at temperature 875 °C (specimen M − 2, Table 2). For understanding of character of deformed microstructure it is important to take into account that temperature plays the main role. It is known that temperature range of austenite and ferrite stability (points A_{C1} and A_{C3}) depends considerably on steel composition. For ferritic-martensitic steel Grade 91 the composition of which is similar to our material the values of A_{C1} and A_{C3} are 818 and 925 °C [34], respectively. To clarify structural state of steel T91 at extrusion temperature of 875 °C a series of experiments was carried out. The specimens of as-received steel were exposed to high temperature during 15 min and subsequently cooled in air. Measurements have showed that in temperature range 825–850 °C a sharp increase of microhardness was observed (Fig. 4).

With further increase of exposure temperature the rate of

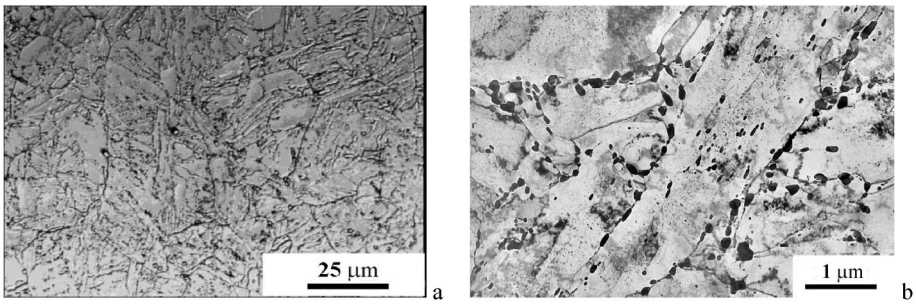

Fig. 2. Microstructure of as-received steel T91: (a) metallography; (b) TEM.

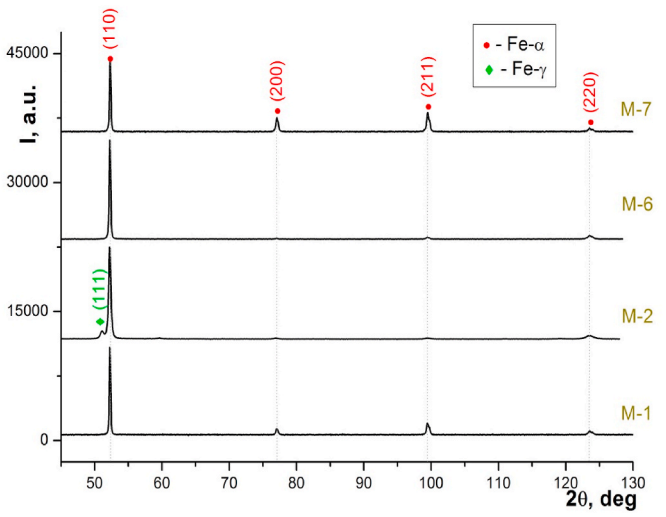

Fig. 3. Diffraction patterns of T91 steel specimens M − 1, M − 2, M − 6 and M-7.

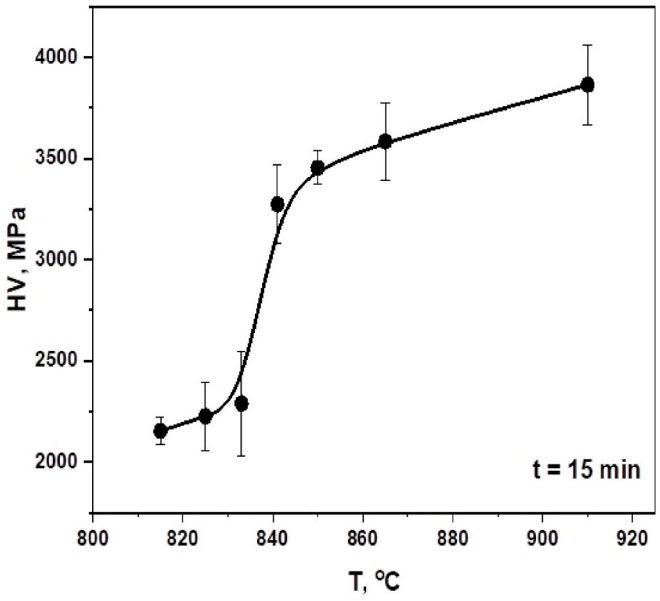

Fig. 4. Dependence of microhardness of steel T91 on exposure temperature during 15 min with the next air cooling.

microhardness increasing reduces. This result and comparison with literature data [34] shows that during extrusion at 875 °C specimen was in two-phase region of existing of austenite and ferrite. Herewith, an austenitic phase was the main one and its transformation into martensitic phase during billet cooling after the extrusion gives the high microhardness values. Martensitic microstructure is confirmed by metallographic (Fig. 5a) and electron-microscopic (Fig. 5b) studies. Together with this, TEM investigations showed considerable differences of billet microstructure from "traditional" martensite with long parallel laths. Microstructure of the steel formed as a result of this operation can be characterized as "defective" or "broken" martensite (Fig. 5b). The cause of such structure formation may be generation of high number of fine subgrains in austenite with rather high degree of disorientation during extrusion. At subsequent cooling below martensite start temperature the subgrain boundaries prevent the formation of "traditional" martensite. In conclusion, obtained microstructure is more similar to usual subgrain microstructure with the mean size of subgrains ~150 nm. But the rectangular shape of "subgrains" and high microhardness of specimen (~3900 MPa) testify to martensite nature of formed microstructure. It can be noted that formation of such "defective" martensite was observed during refinement of as-received austenitic grains as the result of thermal cycling [13].

Because of the low carbon concentration in the steel X-ray diffraction doesn't allow to detect in specimen M − 2 tetragonal distortion of BCC lattice (Fig. 3) parameter of which is $a = 0.28725 \pm 2{\cdot}10^{-5}$ nm, that is higher than corresponding value in as-received state by $\Delta a = 1{\cdot}10^{-4}$ nm. Increase in lattice parameter may be related to dissolution of a part of carbide precipitates at heating to 875 °C and to migration of carbon into austenitic matrix with further formation of supersaturated by carbon martensitic phase under cooling. Crystallite size of martensitic phase is D = 43 nm which is approximately 4 times lower than grains size determined by EM method. In this phase rather high values of microstrain ($\varepsilon = 2.66{\cdot}10^{-3}$) and dislocations density ($\rho = 18.7{\cdot}10^{10}$ cm^{-2}) are observed, that are typical for martensitic microstructure. Also preferred orientation of grains by crystallographic direction <110> along the billet axis is observed. Besides the martensitic phase the billet has the residual austenite Fe-γ (Fig. 3) with axial texture <111>. Fraction of austenite is 19.2%wt, lattice parameter is $a = 0.3591 \pm 2{\cdot}10^{-3}$ nm. The presence of retained austenite in M − 2 sample can be explained as follows. First of all, this sample was extruded at 875 °C (i.e. in two-phase region, as stated above). Local inhomogeneity of composition (by carbon, for example) and/or defective structure of austenite impedes the full transformation of austenite into martensite during the billet cooling. The other samples were deformed in ferritic region and, therefore, do not contain retained austenite, which decay into ferrite and carbides.

Exposure of specimen M − 2 in furnace at 750 °C during 15 min before first upsetting changes considerably microstructure of the steel (Fig. 6 a,b). In the billet recrystallized ferritic grains are formed (Fig. 6a) with the mean size of d_m ~5 μm and coefficient of variation k_v ~0.6. Billets M − 3 with described microstructure were further subjected to deformation by the multiple "upsetting-extrusion".

Fig. 6 b-d represents electron-microscopic images of specimens microstructure after 3, 4 and 5 cycles of "upsetting-extrusion" with decrease of deformation temperature from 750 °C for 1-st cycle to 575 °C for 5-th (Table 2, specimens M − 4, M − 5, M − 6). The nature of

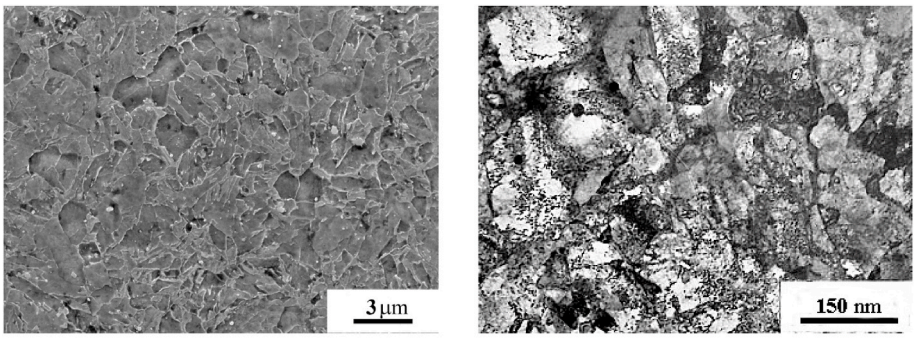

Fig. 5. The microstructure of billet after extrusion at 875 °C: scanning (a) and transmission (b) electron microscopic images.

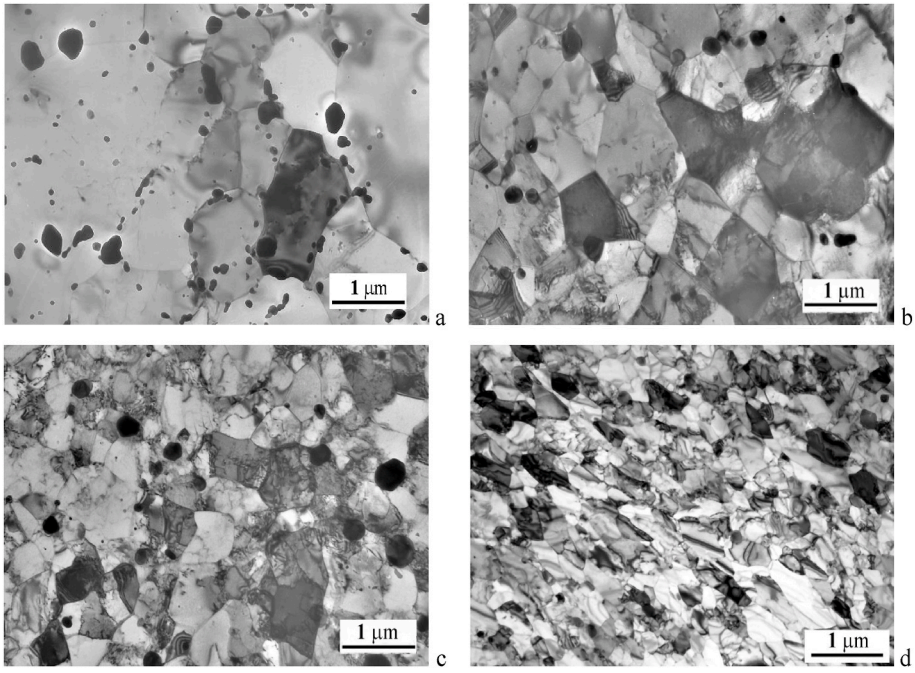

Fig. 6. The microstructure of T91 steel after different treatments: (a) exposed at T = 750 °C during 15 min before SPD, specimen M-3; (b) 3 cycles of "upsetting-extrusion" (UE) at temperatures 750-700-650 °C, e = 4.8, specimen M-4; (c) 4 cycles of UE at temperatures 750-700-650-635 °C, e = 6.4, specimen M-5; (d) 5 cycles of UE at temperatures 750-700-650-635-575 °C, e = 8.0, specimen M-6.

microstructure at different number of cycles is similar – well-formed grained (subgrained) microstructure with contrasting boundaries. Increase in the number of cycles and decrease of "upsetting-extrusion" temperature leads to the considerable decrease in subgrain size (from 5 μm to 145 nm) and to the improving of their size distribution uniformity (coefficient of variation decreases to k_v ~0.5).

Average grain size and microhardness variations of specimens with the increase in the number of cycles are shown in diagram (Fig. 7).

Decrease in mean grain size d_{mg} with the increase in number of UE cycles occurs irregularly. Especially significant microstructure refinement is observed during deformation up to 3 cycles (e = 4.5). Herewith d_{mg} decreases more than 10 times – from 5 μm in as-received state to ~475 nm. With a subsequent increase in number of cycles from 3 to 5 (total deformation e = 8.0) value of d_{mg} decreases approximately in 3 times – from ~475 nm to ~145 nm. It is known that dependence $d_{mg} = d_{mg}(e)$ reaches the saturation with the increase of deformation degree; this can be explained by the processes of recovery and dynamic recrystallization [29].

It is interesting to compare these data with results obtained by the ECAP SPD method [21], moreover, the size of subgrains in as-received specimens was practically the same (≈5 μm). Two passes of ECAP deformation at 700 °C induce the decrease in grain (subgrain) size to 500 nm [21]. Approximately the same grain size (~475 nm) was obtained in our research after 3 cycles of upsetting-extrusion with the decrease of deformation temperature from 750 to 650 °C. Decrease in ECAP temperature to 300 °C led to the decrease in subgrain size to 350 nm [21]. In our case decrease in the UE temperature to 635 and 575 °C during 4-th and 5-th cycles, respectively, allowed to reduce the grain size to 145 nm, that is, more than twice less in comparison with the result in paper [21]. Approximately the same value of grain size (154 nm) was obtained in paper [35] as the results of two passes of ECAP at 300 °C. It should be noted that despite the similarity of deformation conditions the grain size obtained in paper [35] occurred to be 2.3 times lower than in paper [21]. It is probably that such decrease of grain size by ECAP in [35] is due to lower size of as-received grain (2.8 μm vs. 5 μm) or to technological differences of ECAP process not described in article.

Structural characteristics of deformed specimens obtained by XRD analysis are presented in Table 3. All specimens are single-phase and contain Fe-α, except M − 2 where retained austenite is also observed.

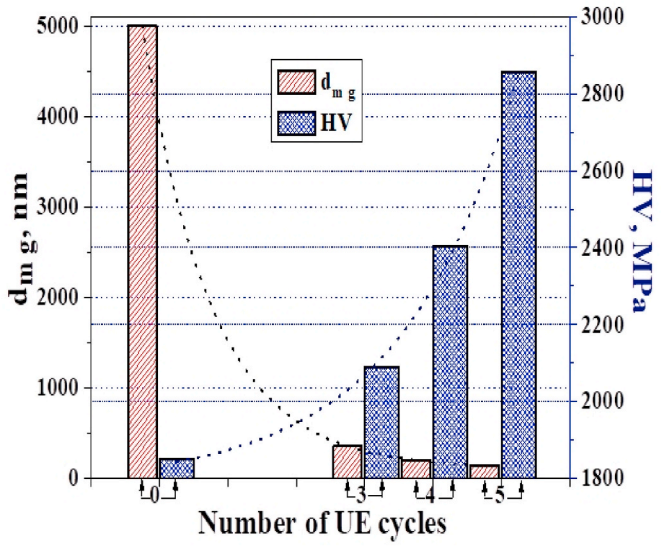

Fig. 7. Dependence of the mean grain size (d_{mg}) and microhardness (HV) of T91 steel with the number of cycles (zero cycle corresponds to the specimen exposed at 750 °C during 15 min).

Increase in number of UE cycles leads to lattice parameter increasing and crystallite size decreasing. At the same time, microstrains and dislocations density rise. The most interesting is the increase in lattice parameter; this may be induced by "deformation dissolution" of carbides precipitates during severe plastic deformation [36]. It is known [13] that the change in BCC lattice parameter of steel Δa is related to the carbon concentration C_c in solid solution by relationship:

$$C_c = 31(\%wt/\text{Å}) \times \Delta a(\text{Å}) \quad (3)$$

Supposing that in matrix of tempered specimen M − 1 the dissolved carbon is practically absent and knowing parameter of matrix lattice $a_{M-1} = 0.28714$ nm we can determine concentration of dissolved carbon in specimen M − 6 as equal to $C_c = 31$ (%wt/Å) × ($a_{M-6} - a_{M-1}$) = 0.053% wt. Thus, after 5 cycles of upsetting extrusion, in matrix of specimen M − 6 approximately half of total carbon concentration in steel T91 is dissolved.

Nature of microhardness changes with the number of deformation cycles is opposite to observed for grain sizes (Fig. 7); a small increase in microhardness for 3 UE cycles (~15%) and considerable increase of microhardness from 3 to 5 cycles (~35%) are detected. Sharp microhardness increase at the last deformation cycles is probably related not only with a decrease in grain size, but also with an increase in quantity of dissolved carbon in ferrite and with the increase in microstrains ε and dislocations density ρ_D (see Table 3).

3.2. Influence of thermal treatment parameters on microstructure and properties of SPD specimens

Thermal treatment of steel after SPD was carried out to optimize microstructure and to determine its stability at elevated temperatures. Investigations were performed on specimens after 5 cycles of UE (specimen M − 6, Table 2). Thermal treatment temperature was 550, 600, 650 and 730 °C, treatment time varied from 1 to 100 h. Preliminary experiments showed that microstructure stabilizes mainly for treatment time of 25 h. Such time was accepted as "basic" one, for which the bulk of research has been carried out. The exception is T = 730 °C: at this temperature thermal treatment was carried out during 1 h and this corresponds to usual regime of T91 steel tempering. As it can be seen from Fig. 8 and Table 4 acceleration of grain growth occurs with the increase of temperature.

So, the lowest grains growth is observed at temperature 550 °C when after exposure during 25h the mean grain size increases in 1.45 times (from 145 to 210 nm) (Fig. 8a). Increase of grain size in 6 times is observed after tempering at 650 °C (Fig. 8c). After tempering at 730 °C for 1h increase of grain size occurs approximately in 7 times (Fig. 8d).

Changes in density and size of secondary phase precipitates occur during thermal treatment apart to changes in grain microstructure. It was found three types of precipitates of different composition, defined as "A", "B" and "C" (see X-ray mapping on Fig. 9). EDS spectra and selected area electron diffractions (SAED) of these precipitates are present in Fig. 10.

Analysis of EDS spectra (Fig. 10 a) showed that there is Cr, Fe, Mo in large, dark-contrasted precipitates type "A" which is typical for $M_{23}C_6$-type carbide precipitates. SAED analysis confirms this (Fig. 10 d). Let us note that in contrast to steel in the tempered martensite state (Fig. 2 a) these precipitates are round-shaped, uniformly distributed in the specimen and present both at grain boundaries and in the grain body.

Finer, grey-contrasted precipitates type "B" are contain more V and less Nb (Fig. 10 b). Contrary, type "C" particles are enriched by Nb with lower content of V (Fig. 10 c). Some of these particles contain a small amount of molybdenum. Such compositions of precipitates type "B" and "C" (Fig. 10 b, c) and diffraction patterns (Fig. 10 e, f) are typical for MX-type carbides/carbonitrides [37,38].

When performing statistical analysis of the average size of precipitates and their density we considered that $M_{23}C_6$ – all precipitates with size exceeding 50 nm, while MX precipitates – with lower size [31–33]. Grain size data, diameter, density and volume fraction of precipitates are presented in Table 4.

It may be concluded that $M_{23}C_6$ precipitates density of SPD samples are practically independent on thermal treatment temperature and their mean size increases a few with the temperature increase. Herewith density of MX precipitates is maximal (2.0×10^{21} 1/m^3) and size of precipitates is minimal (11 nm) after thermal treatment at 550 °C during 25 h. Evolution of structural state of specimens M − 6 at thermal

Table 3
Phase composition and structural characteristics of SPD specimens.

Specimen	Phase	Weight fraction, %wt	Lattice parameter[a] a, nm	Substructural characteristics		
				Crystallite size D/subgrains size, nm	Microstrain ε, 10^{-3}	Dislocations density ρ_D, 10^{10} cm^{-2}
M-1	Fe-α	100	0.28714	112/250–500[b]	1.21	3.3
M-2	Fe-α	80.8	0.28725	43/150	2.66	18.7
	Fe-γ	19.2	0.35910	–	–	–
M-4	Fe-α	100	0.28720	125/475	0.89	2.2
M-5	Fe-α	100	0.28724	105/195	1.71	4.9
M-6	Fe-α	100	0.28731	96/245	1.71	5.4
M − 7[c]	Fe -α	100	0.28718	129/210	1.23	2.9

[a] Error of determining of lattice parameter Fe-α $2{\cdot}10^{-5}$ nm, Fe-γ $2{\cdot}10^{-4}$ nm.
[b] Width of martensitic lath.
[c] Thermal treatment 550 °C/25 h.

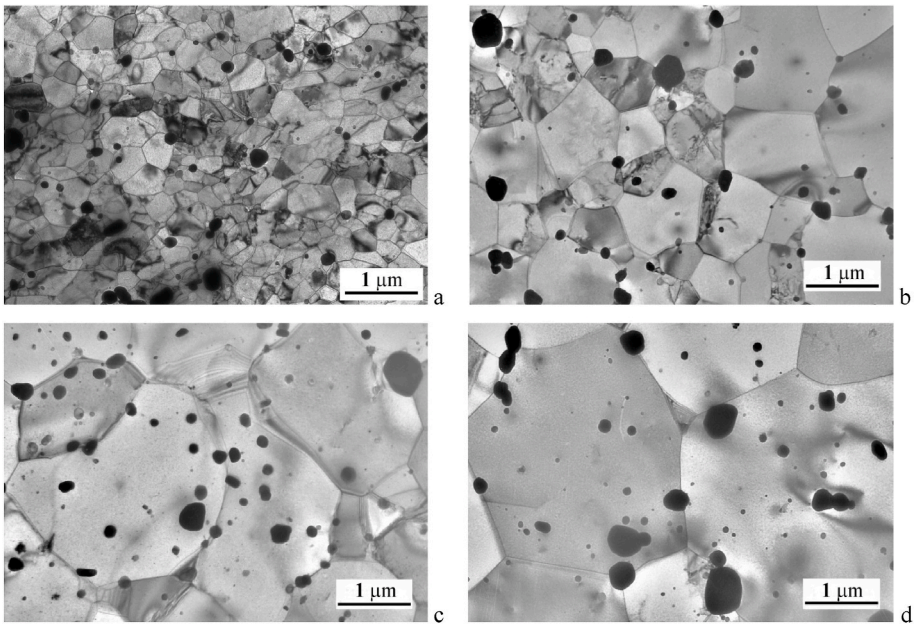

Fig. 8. The microstructure of T91 steel subjected to 5 cycles of UE after different thermal treatments (TT): (a) 550 °C, 25 h, specimen M-7; (b) 600 °C, 25 h, specimen M-8; (c) 650 °C, 25 h, specimen M-9; (d) 730 °C, 1 h, specimen M-10.

Table 4
Parameters of precipitates in steel T91 after 5 cycles of UE and subsequent thermal treatment (TT) according to different regimes (d_{mg} – average grain size, ρ – precipitates density, d_{mf} – precipitates mean diameter, f_V – volume fraction of precipitates).

Specimen	TT regime	d_{mg}, μm	ρ, 1/m^3		d_{mf}, nm		f_V,%	
			$M_{23}C_6$	MX	$M_{23}C_6$	MX	$M_{23}C_6$	MX
M-1	1040°C, 0.5h 730°C, 1 h	20.00	$9.3{\cdot}10^{19}$	$6.5{\cdot}10^{19}$	126	20	7.5	0.3
M-6	–	0.15	$3.4{\cdot}10^{19}$	$2.4{\cdot}10^{20}$	128	15	4.0	0.3
M-7	550°C, 25 h	0.21	$3.6{\cdot}10^{19}$	$2.0{\cdot}10^{21}$	133	11	4.6	1.1
M-8	600°C, 25 h	0.54	$3.0{\cdot}10^{19}$	$5.9{\cdot}10^{20}$	140	16	5.2	0.9
M-9	650°C, 25 h	0.93	$4.2{\cdot}10^{19}$	$1.2{\cdot}10^{20}$	147	28	7.1	0.6
M-10	730°C, 1 h	1.00	$3.5{\cdot}10^{19}$	$1.0{\cdot}10^{21}$	154	15	8.0	1.3

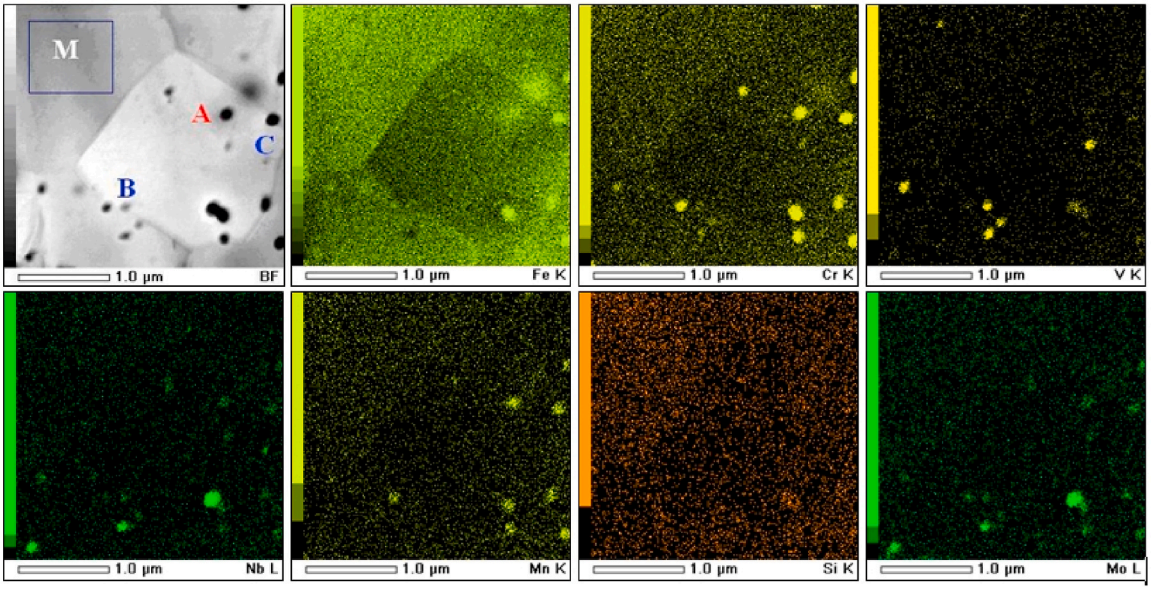

Fig. 9. Elements composition mapping of matrix and precipitates in steel T91 after TT at 650 °C, 25 h. Marks in bright field image: "M" – matrix area, "A"- precipitates [$M_{23}C_6$] type, "B" - [(V, Nb)X] and "C"- [(Nb, V, Mo)X].

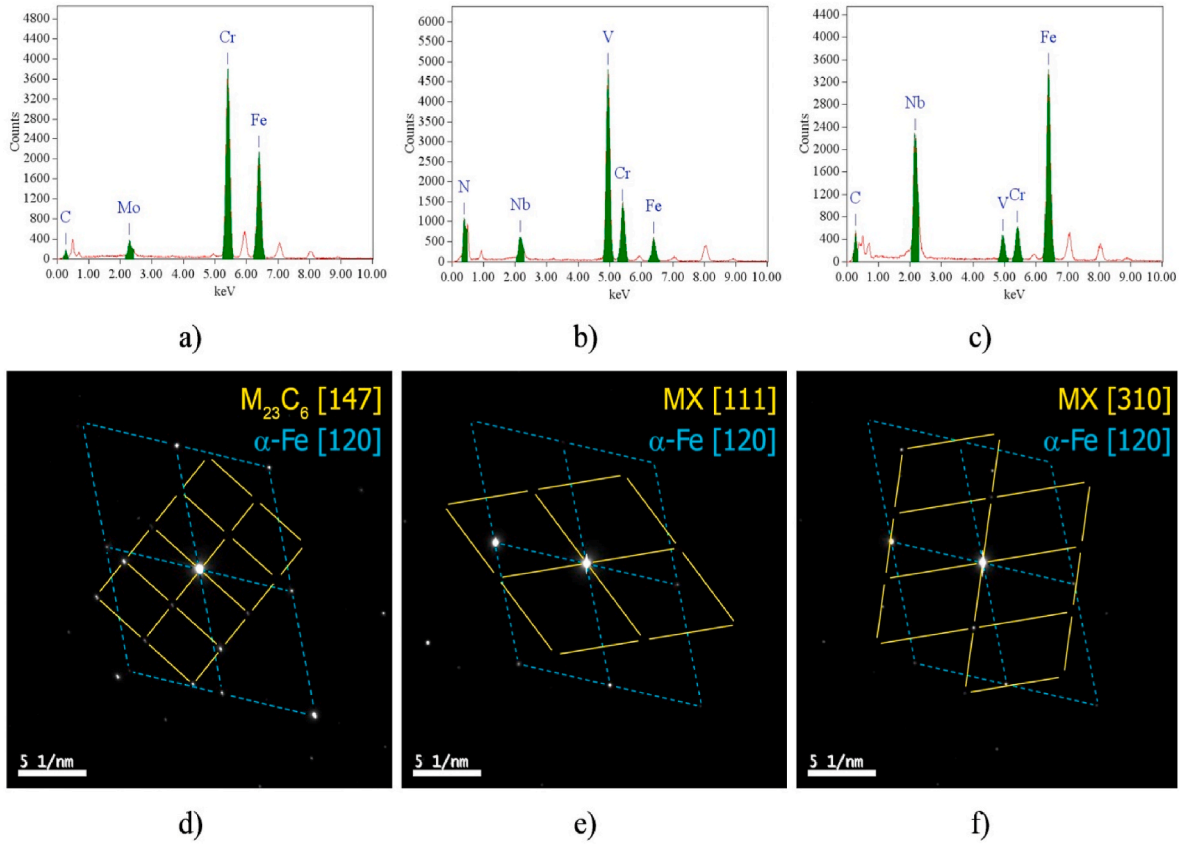

Fig. 10. Identification of precipitates by EDS (a, b, c) and SAED (d, e, f) of typical particles type "A" (a, d), type "B" (b, e) and type "C" (c, f). Diffraction patterns show crystallographic orientation between precipitates (yellow solid lines) and matrix (cyan dash lines).

treatment induces the changes of their microhardness (Table 4 and Fig. 8). In addition the stable value of microhardness in examined range of the thermal treatment time (1–100 h) is observed at TT temperature of 550 °C. What is more for thermal treatment at this temperature during 25 h low increase in microhardness is observed (approximately by 100 MPa) despite the increase in grain size from 145 to 245 nm (Table 4), decrease in dislocation density from 5.4×10^{10} cm^{-2} to 2.9×10^{10} cm^{-2} and decrease in concentration of carbon dissolved into matrix according formula (3) and data in Table 3, from 0.053 to 0.0124%wt. The reason for this is, apparently, the formation of high number of fine MX-type precipitates (Table 4) during thermal treatment, which induce the increase in dispersion hardening. At T = 600 °C and higher the intensive growth of grains occurs (Table 4) also as abrupt decrease in microhardness with the increase in time of thermal treatment (Fig. 11). The effect of dispersion hardening occurs to be insufficient for compensation of strength loss induced by the grain size increase.

Fig. 12 shows Hall-Petch dependencies for microhardness of specimens obtained by upsetting-extrusion with different number of cycles (straight line 1) and as the result of thermal treatment at different temperatures of specimen processed by 5 cycles of UE (straight line 2). It can be seen that line 2 is considerably higher than line 1, that is, with the similar grain sizes microhardness of thermal treated specimens is higher than that of specimens obtained by deformation. This fact is apparently related to the contribution of precipitates of carbide (carbonitride) phases to the strengthening of the grain body. Let us also note the proximity of microhardness values of the specimens subjected to thermal treatment at 650 °C/25h and 730 °C/1h due to the approximate equality of grain size and precipitations parameters (Fig. 12, Table 4).

It should be noted that Hall-Petch coefficients for yield strength determined by data from Fig. 12 (assuming that $\sigma_y \approx 1/3$ HV [21]) are significantly lower than $K_{H-P} \approx 0.43$ GPa•μ$^{-1/2}$ for ECAP processed

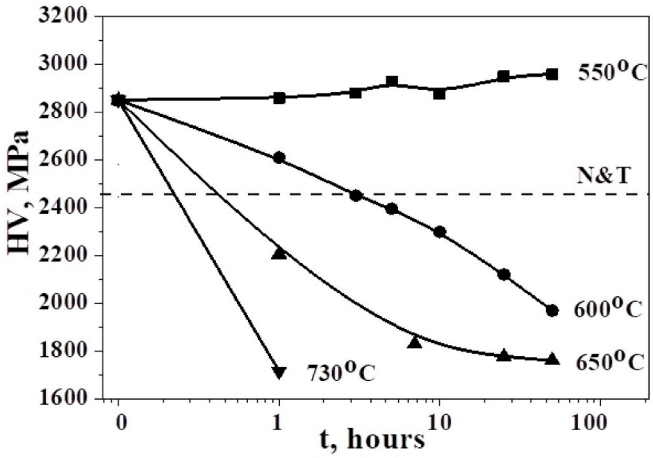

Fig. 11. Dependence of microhardness of specimens subjected to 5 cycles of upsetting-extrusion on time of TT at different temperatures. Dashed line defines the level of microhardness in as-received state (tempered martensite).

samples [21]. Thus, for samples after MUE $K_{H-P} \approx 0.22$ GPa•μ$^{-1/2}$ (Fig. 12, curve 1) and for samples after thermal treatment $K_{H-P} \approx 0.30$ GPa•μ$^{-1/2}$ (Fig. 12, curve 2). The reason for the lowered values of these coefficients may be the small misorientation of the grains formed by this type of TMT. As a result, the grain boundaries become less stoppers for the dislocations movement [35]. An indirect confirmation of the small misorientation of grains can be the increased stability of their sizes during thermal treatment at 550°C, which results in high values of microhardness (Fig. 11). In paper [21,35,36] such stability is observed

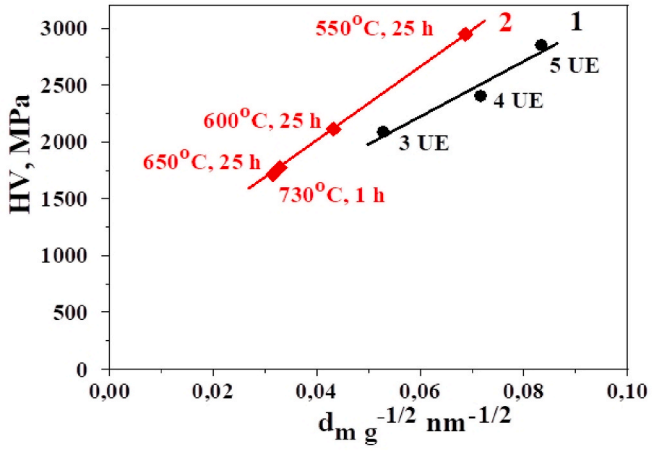

Fig. 12. Hall-Petch dependence of microhardness of specimens produced by deformation with different number of UE cycles (1) and specimens processed by 5 cycles of UE and subsequent thermal treatment at different regimes (2).

at lower temperature (500°C).

Results on tensile tests of specimens in different structural states are presented in Table 5.

The most interesting results are the following: 1) strength characteristics of steel T91 (yield strength $\sigma_{0.2}$ and ultimate tensile strength σ_B) with submicron ferritic microstructure, obtained by SPD and by SPD with subsequent thermal treatment (specimens M − 6, M − 7) exceed characteristics of steel with martensitic microstructure obtained by standard processing "normalization + tempering" (specimen M − 1) in temperature range −196 … +550 °C. Herewith their ductility remains on sufficient level; 2) we revealed for the first time that in specimens of steel T91 with martensitic microstructure with a decrease of testing temperature in range of liquid nitrogen not only strength increases but also ductility improves (rupture elongation δ). For specimens with ferritic microstructure such behavior was not observed. This difference is probably related to the structural features of the martensitic laths boundaries. But further investigation is necessary to explain this effect.

In steels with a martensitic or ferritic microstructure, the yield strength can be estimated by the formula [39]:

$$\sigma_y = \sigma_0 + \sigma_{SS} + \sigma_d + \sigma_p + \sigma_{bs} \quad (4)$$

where σ_0 - friction stress during dislocations movement in iron ($\sigma_0 \sim$ 100 MPa [40,41]); σ_{SS} – solid solution strengthening due to interstitial (carbon) and substitutional atoms; σ_d – dislocation strengthening; σ_p – carbide precipitates strengthening; σ_{bs} – grain boundaries strengthening.

The solid solution strengthening can be estimated by [42]:

$$\sigma_{SS} = 1723[C] + 5.8[Cr] + 18[Mo] + 105[Si] + 45[Mn] + 4.8[V] \quad (5)$$

where σ_{SS} is in MPa and fraction of all elements [Z] is in weight percent.

Dissolution of carbon in the matrix is absent in specimens M − 1 and M − 7, and in specimen M − 6 its concentration is about 0.05% (hardening ~ 360 MPa). Based on the general composition of the steel hardening by substitutional atoms is ~130 MPa. Considering that a significant amount of chromium, molybdenum, manganese, vanadium and niobium is bound in carbides, the actual hardening of the matrix by these elements can be ~70–90 MPa and for all samples (M − 1, M − 6, M − 7) is taken equal to 80 MPa.

Dislocation strengthening:

$$\sigma_d = K_D \cdot \rho_D^{1/2} \quad (6)$$

where $K_D = 7.34 \times 10^{-6}$ MPa m [42]; ρ_D – dislocation density, presented in Table 3.

The precipitation strengthening σ_p is related to the interaction between dislocation and precipitates. Electron microscopic studies have shown [11] that strengthening by nanosized precipitates of MX-carbides is carried out according to the Orowan mechanism (bending around the precipitates by dislocations), while the mechanism of blocking dislocations is characteristic of large $M_{23}C_6$ carbides.

Within the Orowan model [43]:

$$\sigma_{p-MX} = \frac{0.7MGb\sqrt{f_{MX}}}{d_{MX}} \quad (7)$$

where M – Taylor factor ($M \approx 3$); G – shear modulus ($G = 71.85$ GPa [44, 45]); b – Burgers vector ($b = 0.249$ nm).

In model of dispersed barrier hardening (DBH) [46]:

$$\sigma_{p-M23C6} = M\alpha Gb\sqrt{\rho_{M23C6} \cdot d_{M23C6}} \quad (8)$$

where α – barrier strength factor ($\alpha = 0.2$ [44,45]).

For a martensitic microstructure (sample M − 1) the main boundaries contributing to hardening are considered to be the lath boundaries σ_{bsL}.

$$\sigma_{bs} = \sigma_{bsL} = K_L \cdot L^{-1} \quad (9)$$

where $K_L = 115$ MPa μm [42]; L – average lath size ($L = 0.35$ μm for the sample M − 1).

In the case of a ferrite microstructure (samples M − 6, M − 7) the main boundaries are grain (subgrain) boundaries and their contribution σ_{bsg} is described by the Hall-Petch relation:

$$\sigma_{bs} = \sigma_{bsg} = K_{H-P} \cdot d_{mg}^{1/2} \quad (10)$$

where K_{H-P} – Hall-Petch coefficient, d_{mg} – mean grain size.

The values of Hall-Petch coefficient for steel T91, determined from our microhardness data, are $K_{H-P} \approx 0.22$ GPa μm$^{-1/2}$ for samples M − 6 and $K_{H-P} \approx 0.3$ GPa μm$^{-1/2}$ for samples M-7.

Using the above values of various parameters and the data of Tables 3 and 4, the contribution of various mechanisms to the yield stress of samples M − 1, M − 6 and M − 7 were calculated (Table 6).

As can be seen from Table 6, the main contributions to the yield strength give lath boundaries strengthening (in specimens with

Table 5
Mechanical characteristics of T91 steel specimens after different treatments at various test temperatures (T_{test}).

Specimen	T_{test}, °C	$\sigma_{0.2}$, MPa	σ_B, MPa	δ, %
M − 1 (initial)	−196	1189	1242	18.2
	20	728	797	14.5
	550	407	441	13.7
M − 6 (5 cycles of UE)	−196	1370	1430	7.9
	20	853	921	6.1
	550	548	606	9.7
M − 7 (5 cycles of UE + TT 550 °C, 25 h)	−196	1280	1314	7.7
	20	753	911	14.5
	550	513	601	9.7

Table 6
Calculated values of solid solution strengthening σ_{SS}, dislocation strengthening σ_d, carbide precipitates strengthening σ_p, grain boundaries strengthening σ_{bs} and yield strength $\Sigma\sigma_{yi}$ for samples with different microstructure.

Sample values	M-1	M-6	M-7
σ_0, MPa	100	100	100
σ_{ss}, MPa	80	440	80
σ_d, MPa	133	170	125
$\sigma_{p\text{-}MX}$, MPa	75	153	390
$\sigma_{p\text{-}M23C6}$, MPa	37	23	24
σ_{bs}, MPa	328	563	655
$\Sigma\sigma_{yi}$, MPa	**753**	**1449**	**1374**

martensitic microstructure) and grain boundaries strengthening (in specimens with a ferritic microstructure). A significant contribution to the yield strength of steel after SPD is also made by carbon atoms, present in the matrix of samples M − 6 as a result of "mechanical" dissolution. After the thermal treatment of the SPD processed samples approximately the same contribution to the hardening is made by the nanosized MX carbides.

Note that calculated and experimental values of the yield strength for samples M − 1 with martensitic microstructure are quite close (753 MPa and 723 MPa, respectively), while only qualitative agreement is observed for samples M − 6 and M − 7 (see Tables 5 and 6). The calculated values of the yield strength for these samples significantly exceed ones experimentally observed at room temperature. As noted in [41], this may be due to the uncertainty of a number of parameters included in the calculation formulas.

4. Conclusions

1. It is shown that severe plastic deformation (SPD) by the multiple "upsetting-extrusion" method with the decrease of the processing temperature from 750 to 575 °C allowed to obtain mean size of ferritic grains of 145 nm. Two types of precipitates are observed – $M_{23}C_6$ (where M = Cr, Fe, Mo, Mn) and MX (where M = Nb, V; X = C, N). At the same time, particles of both niobium and vanadium prevalence are observed among the MX precipitates.
2. It is determined that increase in number of upsetting-extrusion cycles and decrease in deformation temperature induces not only decrease in grain size and increase in dislocation density but also increase in lattice parameter of ferritic phase. Increase in lattice parameter occurs due to the increase of carbon concentration in ferrite lattice as the result of so-called "deformation dissolution" of carbide precipitates. The consequence of such structural changes is the increase of steel microhardness to 2855 MPa, which is 375 MPa higher than that in as-received steel (state of tempered martensite).
3. We also studied thermal stability of submicron ferritic microstructure obtained by SPD method at temperatures 550–730 °C and time of treatment up to 100 h. It was established that treatment at 550 °C during 25 h increases the mean grains size approximately by 45% (from 145 to 210 nm). Despite such an increase in the grain size, the microhardness rises continuously with an increase in the heat treatment time to 100 h as a result of precipitation hardening due to the formation of a large number of small carbide particles of the MX type (where M = Nb, V; X = C, N). At treatment temperatures of 600 °C and higher the considerable increase of grain size and decrease in microhardness are observed.
4. It is revealed that microhardness dependence on the grain size may be satisfactory described by Hall-Petch relationship both for SPD specimens and specimens after further thermal treatment. Despite the similar grains size microhardness of thermal treated specimens is higher than that of deformed ones due to the dispersion hardening of grain body.
5. Strength characteristics in temperature range −196 … +550 (yield strength $\sigma_{0.2}$ and ultimate tensile strength σ_B) of steel T91 with submicron ferritic microstructure obtained by SPD and by SPD with subsequent thermal treatment exceed characteristics of steel with martensitic microstructure obtained by standard technology "normalization + tempering". Ductility remains on sufficiently high level.
6. The calculations showed that the main contribution to the yield strength of samples with different microstructure is made by boundaries - laths boundaries in samples with a martensitic microstructure and grain boundaries in samples with an ultrafine-grained ferritic microstructure. Strengthening by dissolved carbon atoms and nanosized MX carbides is also significant for certain structural states.
7. Comparison of obtained results with literature data for steel T91 subjected to SPD by torsion under high pressure and equal-channel angular pressing shows that our method of multiple "upsetting-extrusion" allows grain refining and mechanical characteristics improving. Advantage of this method consists in possibility to refine microstructure of billet of industrial size as well as in the simplicity of the mechanical processing.

Datasets related to this article can be found at https://doi.org/10.17632/wg2wwrbwpp.1, an open-source online data repository hosted at Mendeley Data (Rostova, Hanna (2021))

CRediT authorship contribution statement

Victor N. Voyevodin: Conceptualization, Investigation, Visualization, Project administration, Writing – original draft, preparation. **Mikhail A. Tikhonovsky:** Conceptualization, Data curation, Methodology, Writing – original draft, preparation. **Hanna Yu Rostova:** Investigation, Formal analysis, Software, Validation, Writing – original draft, preparation. **Alexander S. Kalchenko:** Investigation. **Igor V. Kolodiy:** Investigation. **Natalya F. Andrievskaya:** Writing – review & editing. **Vladimir S. Okovit:** Investigation. **Marta Serrano:** Resources, Writing – review & editing. **Rebeca Hernandez:** Resources. **Oleksiy M. Velikodnyi:** Investigation. **Anastasia V. Levenets:** Investigation.

Declaration of competing interest

The authors declare that they have no known competing financial interests or personal relationships that could have appeared to influence the work reported in this paper.

Acknowledgments

The work was financially supported by the National Academy of Science of Ukraine (program "Support of the development of main lines of scientific investigations" (KPKVK 6541230)).

References

[1] R.L. Klueh, Ferritic/martensitic steels for advanced, Nuclear Reactors Trans. Indian Inst. Met. 62 (2009) 81–87, https://doi.org/10.1007/s12666-009-0011-3.
[2] K.L. Murty, I. Charit, Structural materials for Gen-IV nuclear reactors: challenges and opportunities, J. Nucl. Mater. 383 (2008) 189–195, https://doi.org/10.1016/j.jnucmat.2008.08.044.
[3] R.L. Klueh, Elevated temperature ferritic and martensitic steels and their application to future nuclear reactors, Int. Mater. Rev. 50 (2005) 287–310, https://doi.org/10.1179/174328005X41140.
[4] R.L. Klueh, A.T. Nelson, Ferritic/martensitic steels for next-generation reactors, J. Nucl. Mater. 371 (2007) 37–52, https://doi.org/10.1016/j.jnucmat.2007.05.005.
[5] M.J. Cohn, J.F. Henry, D. Nass, Fabrication, construction, and operation problems for grade 91 fossil power components, J. Pressure Vessel Technol. 127 (2005) 197–203, https://doi.org/10.1115/1.1904054.
[6] R. Swindeman, M. Santella, P. Maziasz, B. Roberts, K. Coleman, Issues in replacing Cr-Mo steels and stainless steels with 9Cr-1Mo-V steel, Int. J. Pres. Ves. Pip. 81 (2004) 507–512, https://doi.org/10.1016/j.ijpvp.2003.12.009.
[7] X. Zhou, Ch Liu, L. Yu, Y. Liu, H. Li, Phase transformation behavior and microstructural control of high-Cr martensitic/ferritic heat-resistant steels for power and nuclear plants: a review, J. Mater. Sci. Technol. 31 (2015) 235–242, https://doi.org/10.1016/j.jmst.2014.12.001.
[8] M. Tamura, K. Ikeda, H. Esaka, K. Shinozuka, Precipitation behavior of NbC in 9% Cr1%Mo0.2%VNb steel, ISIJ Int. 41 (2001) 908–914, https://doi.org/10.2355/isijinternational.41.908.
[9] U. Rolander, H.-O. Andrén, On atom-probe analysis of cubic MX-type carbides and carbonitrides, J. Phys. Colloq. 49 (C6) (1988), https://doi.org/10.1051/jphyscol:1988652.
[10] Z.J. Yang, K.K. Wang, Y. Yang, Optimization of ECAP—RAP process for preparing semisolid billet of 6061 aluminum alloy, Int. J. Miner. Metall. Mater. 27 (2020) 792–800, https://doi.org/10.1007/s12613-019-1895-5.
[11] J. Zhou, Y. Shen, Y. Hong, W. Xue, R. Misra, Strengthening a fine-grained low activation martensitic steel by nanosized carbides, Mater. Sci. Eng. 769 (2020) 138471, https://doi.org/10.1016/j.msea.2019.138471.
[12] L.M. Wang, Z.B. Wang, K. Lu, Grain size effects on the austenitization process in a nanostructured ferritic steel, Acta Mater. 59 (2011) 3710–3719, https://doi.org/10.1016/j.actamat.2011.03.006.
[13] B.J. Hidalgo, M.S. Santofimia, Effect of prior austenite grain size refinement by thermal cycling on the microstructural features of as-quenched lath martensite,

Metall. Mater. Trans. 47A (№ 11) (2016) 5288–5301, https://doi.org/10.1007/s11661-016-3525-4.
[14] Z.X. Xia, C. Zhang, Z.G. Yang, Control of precipitation behavior in reduced activation steels by intermediate heat treatment, Mater Sci. Eng. A 528 (2011) 6764–6768, https://doi.org/10.1016/j.msea.2011.05.084.
[15] Javier Vivas, Carlos Capdevila, Jose Antonio Jimenez, Miguel Benito-Alfonso, David San-Martin, David San-Martin, Effect of Ausforming Temperature on the Microstructure of G91 Steel, Metals 236 (2017) 1–11, https://doi.org/10.3390/met7070236.
[16] S. Wurster, R. Pippan, Nanostructured metals under irradiation, Scripta Mater. 60 (2009) 1083–1087, https://doi.org/10.1016/j.scriptamat.2009.01.011.
[17] R.A. Andrievskii, Effect of irradiation on the properties of nanomaterials, The physics of metals and metallography 110 (3) (2010) 229–240, https://doi.org/10.1134/S0031918X10090061.
[18] V.K. Shamardin, Y.D. Goncharenko, T.M. Bulanova, A.A. Karsakov, M. M. Abramova, I.V. Alexandrov, M.V. Karavaeva, Effect of neutron irradiation on microstructure and properties of austenitic AISI 321 steel, subjected to equal-channel angular pressing, Rev. Adv. Mater. Sci. 31 (2012) 167–173.
[19] E. Hug, R. Prasath Babu, I. Monnet, A. Etienne, F. Moisy, V. Pralong, N. Enikeev, M. Abramova, X. Sauvage, B. Radiguet, Impact of the nanostructuration on the corrosion resistance and hardness of irradiated 316 austenitic stainless steels, Appl. Surf. Sci. 392 (2016) 1026–1035, https://doi.org/10.1016/j.apsusc.2016.09.110.
[20] M.V. Karavaeva, M.A. Nikitina, A.V. Ganeev, R.K. Islamgaliev, High-strength state of ultrafine-grained martensitic steel produced by high pressure torsion, IOP Conf. Ser. Mater. Sci. Eng. 179 (2017) 1–9, https://doi.org/10.1088/1757-899X/179/1/012037, 012037.
[21] D.C. Foley, K.T. Hartwig, S.A. Maloy, P. Hosemann, X. Zhang, Grain refinement of T91 alloy by equal channel angular pressing, J. Nucl. Mater. 389 (2009) 221–224, https://doi.org/10.1016/j.jnucmat.2009.02.005.
[22] Z.Q. Fan, T. Hao, S.X. Zhao, G.N. Luo, C.S. Liu, Q.F. Fang, The microstructure and mechanical properties of T91 steel processed by ECAP at room temperature, J. Nucl. Mater. 434 (2013) 417–421, https://doi.org/10.1016/j.jnucmat.2012.12.009.
[23] Sh Chen, X. Jin, L. Rong, Improving the strength and ductility of reduced activation ferritic/martensitic steel by cold-swaging and post-annealing, Mater. Sci. Eng. 631 (2015) 139–143, https://doi.org/10.1016/j.msea.2015.02.044.
[24] I.I. Papirov, G.F. Tikhinskiy, Structure and mechanical properties of fine-grained deformed beryllium, Physics of metals and metal science 29 (5) (1970) 1057–1060 (in Russian).
[25] O.V. Chorniy, Ya.D. Starodubov, O.I. Volchok, G.E. Storozhilov, Patent 42487 A Ukraine, МПК 7 H01B12/00 "Method for Manufacturing Niobium-Titanium Superconductor" Bulletin N№ 9, Publ., 2001, 15.10.2001. (in Ukrainian).
[26] V.M. Azhazha, O.V. Chorniy, G.E. Storozhilov, N.F. Andriyevskaya, T. Yu Rudycheva, Study of the deformed state during multidirectional processing of Nb-Ti alloy, Problems of Atomic Sci. Technol. 6 (14) (2004) 136–139 (in Russian).
[27] G.E. Storozhilov, I.N. Shapoval, O.V. Chorniy, N.F. Andriyevskaya, Study of the structure size distribution during thermomechanical processing of niobium-titanium alloy, Problems of Atomic Sci. Technol. 1 (15) (2006) 67–71 (in Russian).
[28] O.V. Chernyi, G.E. Storozhilov, N.F. Andrievskaya, V.O. Ilicheva, YaD. Starodubov, O.I. Volchok, L.A. Chirkina, M.B. Lazareva, V.S. Okovit, Structure and properties of differently directed deformed niobium-titanium alloy, IEEE Trans. Appl. Supercond. 15 (2) (2005) 3502–3505.
[29] N.F. Andriyevskaya, V.S. Okovit, T.Yu Rudycheva, M.P. Starolat, G.E. Storozhilov, M.A. Tikhonovsky, P.A. Khaimovich, I.N. Shapoval, Evolution of the structure and properties of the NT-50 alloy at large plastic deformations, Physics and High Pressure Technology 19 (2) (2009) 136–142 (in Russian).
[30] H.P. Klug, L.E. Alexander, X-ray Diffraction Procedures for Polycrystalline and Amorphous Materials, second ed., John Wiley & Sons, New York-Sydney-Toronto, 1974, ISBN 978-0-471-49369-3, p. 992.
[31] F. Abe, S. Nakazawa, H. Araki, T. Noda, The role of microstructural instability on creep behaviour of a low radioactivation martensitic 9Cr-2 W steel Metal, OR Trans. 23 (1992) 469–477, https://doi.org/10.1007/BF02801164.
[32] M. Tamura, H. Hayakawa, M. Tanimura, A. Hishinuma, T. Kando, Development of potential low activation ferritic and austenitic steels, J. Nucl. Mater. 141–143 (1986) 1067–1073, https://doi.org/10.1016/0022-3115(86)90144-3.
[33] M. Tamura, K. Ikeda, H. Esaka, K. Shinozuka, Precipitation behavior of NbC in 9% Cr1%Mo0.2%VNb steel, ISIJ Int. 41 (2001) 908–914, https://doi.org/10.2355/isijinternational.41.908.
[34] B. Silwal, L. Li, A. Deceuster, B. Griffiths, Effect of postweld heat treatment on the toughness of heat-affected zone for grade 91 steel, Weld. J. 92 (2013), p. 80-s – 87-s.
[35] M. Song, R. Zhu, D.C. Foley, C. Sun, Y. Chen, K.T. Hartwig, X. Zhang, Enhancement of strength and ductility in ultrafine-grained T91 steel through thermomechanical treatments, J. of Mat. Science 48 (2013) 7360–7373, https://doi.org/10.1007/s10853-013-7522-3.
[36] T. Hao, Z.Q. Fan, S.X. Zhao, G.N. Luo, C.S. Liu, Q.F. Fang, Strengthening mechanism and thermal stability of severely deformed ferritic/martensitic steel, Mat. Science & Engineering 596 (2014) 244–249, https://doi.org/10.1016/j.msea.2013.12.062.
[37] U. Rolander, H.-O. Andrén, On atom-probe analysis of cubic MX-type carbides and carbonitrides, J. Phys. Colloq. 49 (C6) (1988), https://doi.org/10.1051/jphyscol:1988652. C6-299-C6-304.
[38] X. Zhou, Ch Liu, L. Yu, Y. Liu, H. Li, Phase transformation behavior and microstructural control of high-Cr martensitic/ferritic heat-resistant steels for power and nuclear plants: A Review, J. Mater. Sci. Technol. 31 (2015) 235–242, https://doi.org/10.1016/j.jmst.2014.12.001.
[39] M. Song, C. Sun, Z. Fan, Y. Chen, R. Zhu, K. Yu, K. Hartwig, H. Wang, X. Zhang, A roadmap for tailoring the strength and ductility of ferritic/martensitic T91 steel via thermo-mechanical treatment, Acta Mater. 112 (2016) 361–377, https://doi.org/10.1016/j.actamat.2016.04.031.
[40] S. Takaki, K. Kawasaki, Y. Kimura, Mechanical properties of ultra fine grained steels, J. Mater. Process. Technol. 117 (2001) 359–363, https://doi.org/10.1016/S0924-0136(01)00797-X.
[41] B. Han, F. Mohamed, E. Lavernia, Mechanical properties of iron processed by severe plastic deformation, Metall. Mater. Trans. 34 (2003) 71–83, https://doi.org/10.1007/s11661-003-0209-7.
[42] H. Bhadeshia, R. Honeycombe, Steels: Microstructure and Properties, Butterworth-Heinemann, 2011, ISBN 9780081002704, p. 488.
[43] G.E. Lucas, The evolution of mechanical property change in irradiated austenitic stainless steels, J. Nucl. Mater. 206 (1993) 287–305, https://doi.org/10.1016/0022-3115(93)90129-M.
[44] G. Gupta, G. Was, Improved creep behavior of ferritic-martensitic alloy T91 by subgrain boundary density enhancement, Metall. Mater. Trans. 39 (2008) 150.
[45] K. Maruyama, K. Sawada, J. Koike, Strengthening mechanisms of creep resistant tempered martensitic steel, ISIJ Int. 41 (6) (2001) 641–653, https://doi.org/10.1007/s11661-007-9411-3.
[46] K. Cho, S. Park, D. Choi, H. Kwon, Influence of Ti addition on the microstructure and mechanical properties of a 5% Cr-Mo-V steel, J. Alloys Compd. 626 (2015) 314–322, https://doi.org/10.1016/j.jallcom.2014.12.040.